

Relaxation Dynamics of Photoexcited Excitons in Rubrene Single Crystals Using Femtosecond Absorption Spectroscopy

S. Tao,¹ N. Ohtani,¹ R. Uchida,¹ T. Miyamoto,¹ Y. Matsui,¹ H. Yada,¹ H. Uemura,¹ H. Matsuzaki,^{1,*} T. Uemura,² J. Takeya,² and H. Okamoto^{1,†}

¹Department of Advanced Materials Science, University of Tokyo, Kashiwa, Chiba 277-8561, Japan

²Institute of Scientific and Industrial Research, Osaka University, Ibaraki 567-0047, Japan

(Received 24 October 2011; revised manuscript received 6 April 2012; published 30 August 2012)

The relaxation dynamics of an exciton in rubrene was investigated by femtosecond absorption spectroscopy. Exciton relaxation to a self-trapped state occurs via the coherent oscillation with 78 cm^{-1} due to a coupled mode of molecular deformations with phenyl-side-group motions and molecular displacements. From the temperature dependence of the decay time of excitons, the energy necessary for an exciton to escape from a self-trapped state is evaluated to be $\sim 35\text{ meV}$ ($\sim 400\text{ K}$). As a result, a self-trapped exciton is stable at low temperatures. At room temperature, excitons can escape from a self-trapped state and, subsequently, they are dissociated to charged species. The exciton dissociation mechanism is discussed on the basis of the results.

DOI: 10.1103/PhysRevLett.109.097403

PACS numbers: 78.47.jb, 72.20.Jv, 78.40.-q, 78.47.D-

Rubrene is an important material for organic field effect transistors (FETs) because of its highest mobility among organic molecular semiconductors [1–3]. The Hall-effect measurements suggest a band transport mechanism [4,5]. In addition, a potential of rubrene as a photoconductive and light-emitting material has also been attracting much attention [6–8]. When we consider the applications of molecular semiconductors to optical devices, it is important to clarify the nature of a molecular exciton. In the present study, we focus on the relaxation dynamics of an exciton in rubrene.

Rubrene is a derivative of tetracene with four phenyl side groups [Fig. 1(a)]. The characters of molecular orbitals in isolated rubrene and tetracene molecules are similar to each other [9]. However, their crystal structures are significantly different. The crystal structure of rubrene projected on the **ab** plane is shown in the inset of Fig. 1(b). Tetracene backbones are aligned in a slipped-cofacial configuration, forming a π -stacking structure along the **b** axis. This results in the large mobility $\mu(>20\text{ cm}^2/\text{Vs})$ along **b** [4,5]. In tetracene, such a π -stacking structure is not formed and $\mu(\sim 2\text{ cm}^2/\text{Vs})$ is much lower [10]. Photoluminescence (PL) properties of tetracene and rubrene are also considerably different from each other; in tetracene, both free excitons (FEs) and self-trapped excitons (STEs) were identified [11,12], while in rubrene only the PL peak (2.18 eV) with a large Stokes shift ($\sim 140\text{ meV}$) was observed [6], suggesting the formation of STEs [13]. More recently, we reported photoinduced absorption (PA) spectra due to excitons and photocarriers in rubrene by femtosecond (fs) pump-probe (PP) spectroscopy and suggested that an exciton is dissociated to charged species [13]. This is a special property which is not seen in other molecular semiconductors [14,15]. However, it has not been fully understood yet.

Here, we investigated temperature dependences of PA signals due to excitons and charged species. At low temperatures, we observed a coherent oscillation on the PA signals of excitons. This oscillation was assigned to a

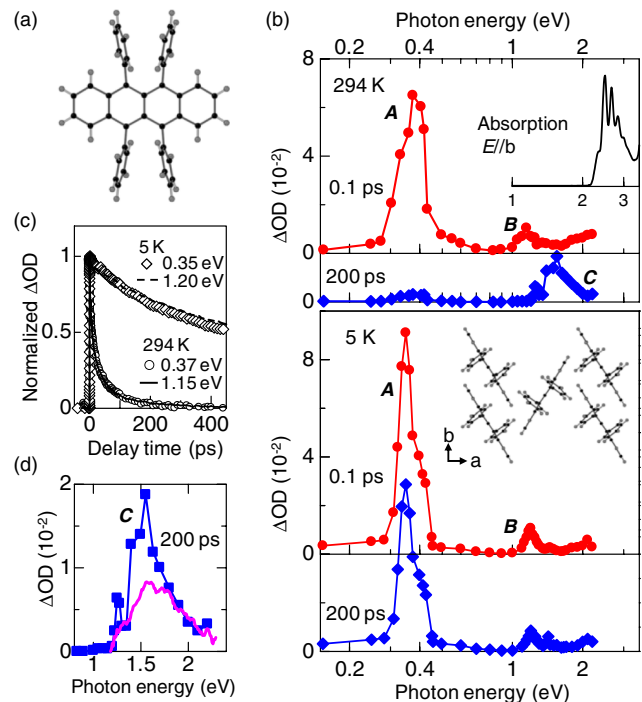


FIG. 1 (color online). (a) Molecular structure of rubrene. (b) ΔOD spectra of rubrene on the **ab** plane with the pump and probe pulses polarized $//\mathbf{b}$. The pump energy was 2.23 eV at 294 K and 2.27 eV at 5 K. In the upper panel, the thin solid line shows the absorption spectrum ($E//\mathbf{b}$). (c) Time evolutions of PA bands **A** and **B**. (d) Expanded PA band **C** at 294 K. The thick solid line shows the FIA [18].

coupled mode of molecular deformations and displacements, which stabilizes excitons as STEs. In addition, we found that the exciton dissociation process is characterized by the small activation energy of 35 meV. The exciton dissociation mechanism will be discussed on the basis of the results.

Single crystals of rubrene were grown by physical vapor transport in a stream of argon gas. They show high mobility larger than $10 \text{ cm}^2/\text{Vs}$ in FETs. The PL spectrum at 10 K showed the intrinsic peak at 2.18 eV, which is presented in the Supplemental Material [16]. This demonstrates that the sample quality is high enough. In the PP spectroscopy, we used two systems with a time resolution T_r of 180 and 36 fs, both of which were based on a Ti:Al₂O₃ regenerative amplifier (785 nm, the duration of 130 fs, and the repetition rate of 1 kHz). In the system with $T_r = 180$ fs, the output from the amplifier was divided into two beams, which were used as excitation sources for two optical parametric amplifiers (OPAs). From these OPAs, pump and probe pulses were obtained. In the system with $T_r = 36$ fs, two noncollinear OPAs were excited by the outputs from the regenerative amplifier, and pump and probe pulses with the duration of ~ 20 fs were obtained. The delay time t_d of the probe pulse relative to the pump pulse was controlled by changing the pump path length. The excitation photon density was adjusted to be smaller than 10^{-3} photon/molecule.

The absorption (optical density: OD) spectrum of rubrene measured on the **ab** plane with the electric field of lights $\mathbf{E} // \mathbf{b}$ is shown in the upper part of Fig. 1(b). The structure at 2.32 eV and the peaks on the higher-energy side are a zero-phonon line of the lowest exciton and its phonon side bands, respectively [6,7]. PA (ΔOD) spectra at 294 and 5 K by the excitation of the lowest exciton measured with $T_r = 180$ fs are shown in Fig. 1(b). Polarizations of pump and probe pulses were $// \mathbf{b}$. Just after the photoirradiation, two peaks (**A** and **B**) were observed at ~ 0.37 and ~ 1.15 eV, respectively. Their time evolutions were the same with each other [Fig. 1(c)] [13], suggesting that both **A** and **B** were due to STEs.

The spectral shapes of ΔOD at 294 and 5 K are almost the same at $t_d = 0.2$ ps; however, their temporal evolutions are significantly different. At 294 K, **A** and **B** almost disappeared at $t_d = 200$ ps. Instead, a broad band **C** becomes dominant, which was attributed to the superposition of induced absorptions of positively and negatively charged species [13,17]. This assignment was also supported by the field-induced absorption (FIA) due to hole carriers in FETs [the thick solid line in Fig. 1(d)] [18]. The FIA is overlapped on band **C**. The difference between band **C** and the FIA is attributable to the absorption due to negatively charged molecules [13].

At 5 K, the decay of bands **A** and **B** becomes very slow. At 200 ps, ΔOD at around 1.5 eV slightly increases but the overall shape of ΔOD is almost the same with that at 0.2 ps.

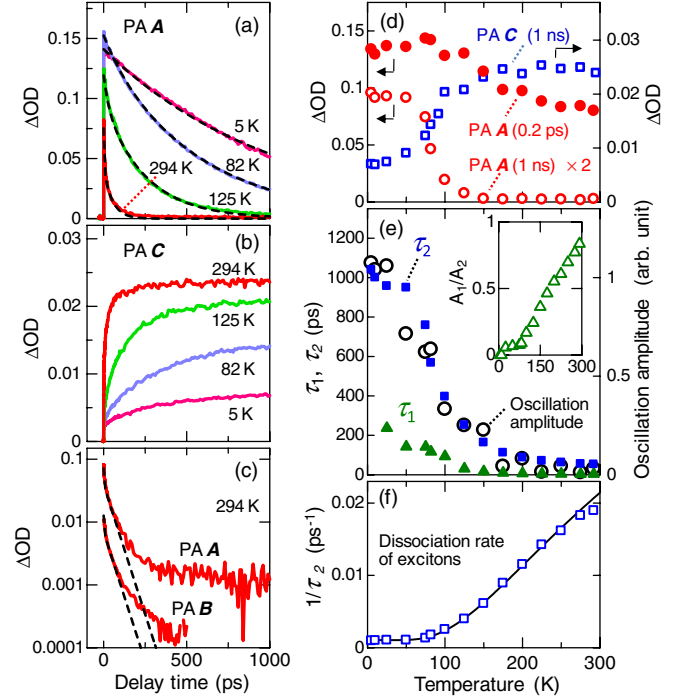


FIG. 2 (color online). Time evolutions of (a) PA band **A** and (b) PA band **C**. The dashed lines in (a) are fitting curves by Eq. (1). (c) Time evolutions of **A** and **B** at 294 K. (d) Temperature dependences of **A** at 0.2 ps and 1 ns and of **C** at 1 ns. (e) Temperature dependences of the exciton decay times τ_1 and τ_2 , the amplitude of coherent oscillation with 78 cm^{-1} , and A_1/A_2 (inset). (f) Exciton decay rate $1/\tau_2$. The solid line shows the fitting curve by Eq. (3).

In Figs. 2(a) and 2(b), we show the temperature dependences of the time evolutions of band **A** (0.37 eV) reflecting exciton dynamics and band **C** (1.55 eV) reflecting the carrier dynamics. With decreasing temperature, both the decay time of excitons and the generation time of carriers increase in the same manner, suggesting that the exciton decay is related to the generation of charged species. This picture is also ascertained from the temperature dependence of the PA intensities. As shown in Fig. 2(d), band **A** (0.37 eV) due to excitons at 0.2 ps is not changed so much in the whole temperature region, while that at 1 ns gradually increases with decrease of temperature from 150 K and becomes almost constant below 50 K. Band **C** (1.55 eV) due to charged species at 1 ns, rather, decreases below 150 K. These results suggest that a finite potential barrier exists when an exciton escapes from an STE to a path for the dissociation. This point is discussed again later.

To obtain more quantitative information about the exciton decay (or dissociation), we analyzed the time evolutions of ΔOD at the peak of band **A** for various temperatures [Fig. 2(a)], using the following formula:

$$\Delta\text{OD} = A_1 \exp\left(-\frac{t}{\tau_1}\right) + A_2 \exp\left(-\frac{t}{\tau_2}\right); (\tau_1 < \tau_2). \quad (1)$$

The fitting results are shown by the dashed lines in Fig. 2(a), which reproduce well the experimental results. The temperature dependences of τ_1 , τ_2 , and A_1/A_2 are shown in Fig. 2(e). The physical meanings of the two terms in Eq. (1) are also discussed later.

Next, we discuss the primary relaxation dynamics of excitons by scrutinizing the time evolutions of bands **A** and **B** at 5 K [Fig. 3(a)]. Oscillatory structures were observed on ΔOD for **A** and **B** in common. In Fig. 3(a), dashed lines were drawn from $t_d = 0$ ps with the same time interval (0.21 ps) and correspond well to the peaks or dips of the oscillatory components. This suggests that the oscillation is of the cosine type and generated by a displacive-excitation mechanism [19,20] and that the exciton is relaxed via a specific phonon mode with the period of 0.42 ps (the frequency of 78 cm^{-1}).

Previous steady-state [21] and stimulated [22] Raman spectroscopy revealed that several Raman bands exist below 200 cm^{-1} . Among them, a strong band exists at 76 cm^{-1} , which is nearly equal to the coherent oscillation frequency. This band was assigned to a mode arising from the mixing between a lattice mode (molecular displacements) and an intramolecular mode, including the motions of phenyl side groups [Fig. 4(a)] [21,23].

To clarify the physical picture of the coherent oscillation, we subtracted background components from ΔOD of bands **A** and **B** at 5 K [Fig. 3(a)] for various probe energies and analyzed the residual oscillatory components (OSC) ΔOD_{OSC} by using $\Delta OD_{\text{OSC}} = A_3 \cos(\omega t) \exp(-t/\tau_3)$. Each oscillatory component was well reproduced by this formula (not shown). Oscillation amplitudes A_3 for **A** and **B** are plotted by triangles in Figs. 3(b) and 3(c), respectively, together with the PA spectra (circles). In both **A** and **B**, A_3 is positive in the lower-energy side of the peak and

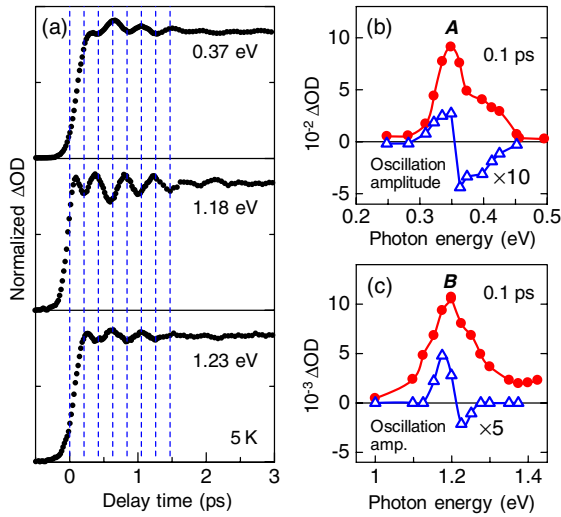


FIG. 3 (color online). (a) Time evolutions of PA signals in rubrene (2.27 eV pump) at 5 K. (b),(c) PA spectra (circles) and oscillation amplitudes (triangles) in (b) PA band **A** and (c) PA band **B** at 5 K (see the text).

negative in the higher-energy side, indicating that the 78 cm^{-1} mode initially increases the PA energies and gives rise to their subsequent periodic modulations. This demonstrates that the 78 cm^{-1} mode stabilizes excitons and is responsible for the STE formation. The STE formation and coherent oscillation are illustrated in Fig. 4(b).

To investigate the exciton relaxation dynamics in more detail, we performed PP measurements with $T_r = 36$ fs. The lowest probe energy in this PP system is 0.75 eV, so we focused on the higher-energy band **B** at ~ 1.15 eV. We showed spectra of the pump and probe pulses in the inset of Fig. 4(c) together with the absorption spectrum at 10 K. They were broad, so the observed time evolution reflects the averaged dynamics of **B**. Time evolution of ΔOD at 5 K is shown in Fig. 4(c). We fit Eq. (2) to the time evolution:

$$\Delta OD = A_0 \exp\left(-\frac{t}{\tau_0}\right) + A_2 \exp\left(-\frac{t}{\tau_2}\right) + A_3 \cos(\omega t) \exp\left(-\frac{t}{\tau_3}\right). \quad (2)$$

The first term of Eq. (1) can be neglected at low temperatures [the inset of Fig. 2(e)]. The calculated time evolution with $\tau_0 = 77$ fs, $\tau_2 = 1.0$ ns, and $\tau_3 = 1.1$ ps [solid line in Fig. 4(c)] reproduced well the experimental one. Each term is shown in Fig. 4(d). The first term in Eq. (2) is attributable to the relaxation process from FEs to STEs. The second term is due to the decay of STEs. The decay

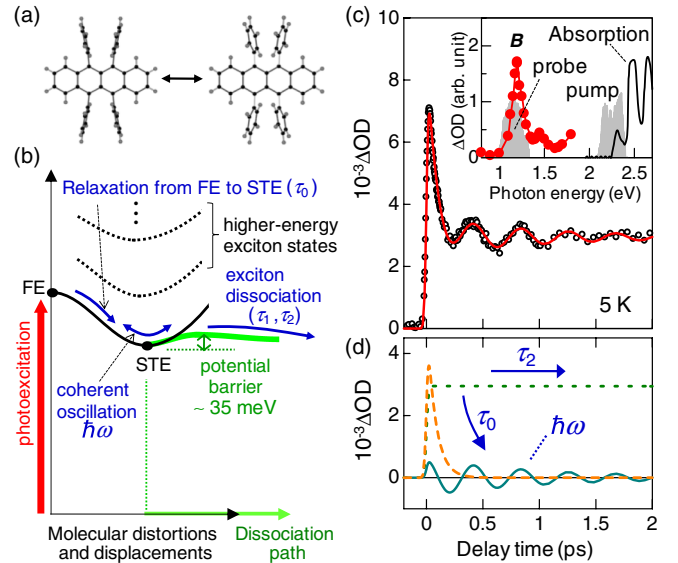


FIG. 4 (color online). (a) Phenyl-side-group motions expected in the exciton relaxation [21]. (b) Schematic of exciton relaxation processes. (c) Time evolution of PA band **B** at around 1.2 eV measured with $T_r = 36$ fs. The solid line represents the fitting curve by Eq. (2). The inset shows spectra of the pump and probe pulses (shades), PA band **B** at 0.2 ps (5 K) (circles), and the absorption spectrum (10 K). (d) Three components of the fitting curve in (c).

time $\tau_2 (= 1.0 \text{ ns})$ is very long, giving the constant background in Fig. 4(c). The third term shows the coherent oscillation with 78 cm^{-1} . No higher-frequency oscillations were observed, supporting the dominant role of the 78 cm^{-1} mode on the STE formation.

Here, let us go back to the temperature dependence of the exciton decay. As shown in the inset of Fig. 2(e), the main term of the decay is the second term of Eq. (1) characterized by τ_2 . We plotted in Fig. 2(f) the temperature dependence of the exciton decay rate $1/\tau_2$, which was reproduced by the sum of a constant term and a thermal activation process [Eq. (3)], as shown by the solid line in Fig. 2(f):

$$\frac{1}{\tau_2} = \frac{1}{\tau_T} + \frac{1}{\tau_A} \exp\left(-\frac{\Delta}{kT}\right). \quad (3)$$

The parameters used were $\tau_T = 1.0 \text{ ns}$, $\tau_A = 13.3 \text{ ps}$, and $\Delta = 35 \text{ meV}$. Δ is considered to be an energy barrier between an STE and a path for the dissociation, as is illustrated in Fig. 4(b). Δ is much smaller than the binding energy of an FE ($\sim 0.4 \text{ eV}$) [13].

In Fig. 2(e), we plotted the oscillation amplitude A_3 against temperature, together with the decay time τ_2 of excitons. Two quantities show almost the same temperature dependence with band *A* at 1 ns and the opposite temperature dependence with band *C* at 1 ns, as is shown in Fig. 2(d). These results suggest that the STE formation by the 78 cm^{-1} mode competes with the exciton decay, which is related to the carrier generation. It is, therefore, natural to consider that the time constants τ_1 and τ_2 correspond to the decay time of an exciton during the lattice relaxation of an FE and that of an STE, respectively.

Now, we discuss the mechanism for the exciton decay and the carrier generation by taking the previous studies into account. The PL studies suggested that excitons survive for $t_d > 1 \text{ ns}$ at room temperature [24,25]. To obtain information of excitons for $t_d > 200 \text{ ps}$, we show in Fig. 2(c) the time evolutions of *A* and *B* in a logarithmic scale. For $t_d > 200 \text{ ps}$, data deviate from Eq. (1) (dashed lines) and show the presence of long-lived excitons, consistent with the previous PL studies. The long-lived excitons might be related to the fission and fusion processes between a singlet exciton (S_1) and a pair of triplet excitons ($T_1 + T_1$) [8,26]. However, our present PA dynamics and previously reported picosecond PL dynamics [13] clearly show that most excitons decay up to $t_d \sim 200 \text{ ps}$ at room temperature.

Najafov *et al.* proposed that the fission of S_1 to $2T_1$ and the dissociation of T_1 to carriers after their diffusion to a crystal surface play dominant roles in the surface photoconductivity [8]. In tetracene, the long-lived absorption of T_1 generated by the fission of S_1 was indeed observed at $\sim 1.7 \text{ eV}$ and the energy for the fission process was evaluated to be $\sim 70 \text{ meV}$ [27]. In rubrene, on the other hand, long-lived band *C* is due to charged species. Although the absorption depth of the pump pulse ($\sim 2.2 \text{ eV}$) is long ($\sim 9 \mu\text{m}$), a large part of *C* appears within 50 ps after

photoexcitation [13]. This suggests that the main part of photocarriers responsible for *C* is not generated at the surface but generated in the bulk [28].

From these discussions, we can expect two possible scenarios for the exciton dissociation. The first one is the impurity-induced dissociation [6]. In rubrene, electron traps are considered to exist even in high-quality single crystals. An exciton which escapes from an STE by gaining the energy can encounter an electron trap. Then, it may be dissociated to a hole carrier and a trapped electron. Another scenario is that electron and hole carriers are stabilized by polaronic effects and they can be created from an STE [13]. In this case, Δ corresponds to the barrier between a self-trapped S_1 and a polaron pair (P^+ and P^-). In this scenario, however, we cannot exclude a possibility that a polaron pair is generated from a T_1 pair via a sequence of reactions ($S_1 \rightarrow 2T_1 \rightarrow P^+ + P^-$). When the latter process is much faster than the former, T_1 is difficult to detect. In this case, Δ corresponds to the energy necessary for S_1 to be dissociated to a T_1 pair. To clarify the exciton dissociation mechanism and the role of T_1 , further studies should be necessary.

In summary, in rubrene, excitons are stabilized as STEs with the decay time of $\sim 1 \text{ ns}$ at low temperatures. The coupled mode of molecular deformations with phenyl-side-group motions and molecular displacements is responsible for the STE formation. At room temperature, STEs decay within 200 ps and are converted to charged species. The potential barrier for the exciton dissociation is very small, being $\sim 35 \text{ meV}$. Thus, the unique dissociation paths of excitons exist in rubrene, differently from other molecular semiconductors.

This work has been partly supported by MEXT, Japan (No. 20110005).

*Present address: Research Institute of Instrumentation Frontier, National Institute of Advanced Industrial Science and Technology (AIST), Ibaraki 305-8565, Japan.
†okamoto@k.u-tokyo.ac.jp

- [1] V. C. Sundar, J. Zaumseil, V. Podzorov, E. Menard, R. L. Willett, T. Someya, M. E. Gershenson, and J. A. Rogers, *Science* **303**, 1644 (2004).
- [2] V. Podzorov, E. Menard, A. Borissov, V. Kiryukhin, J. A. Rogers, and M. E. Gershenson, *Phys. Rev. Lett.* **93**, 086602 (2004).
- [3] J. Takeya, M. Yamagishi, Y. Tominari, R. Hirahara, Y. Nakazawa, T. Nishikawa, T. Kawase, T. Shimoda, and S. Ogawa, *Appl. Phys. Lett.* **90**, 102120 (2007).
- [4] J. Takeya, K. Tsukagoshi, Y. Aoyagi, T. Takenobu, and Y. Iwasa, *Jpn. J. Appl. Phys.* **44**, L1393 (2005).
- [5] V. Podzorov, E. Menard, J. A. Rogers, and M. E. Gershenson, *Phys. Rev. Lett.* **95**, 226601 (2005).
- [6] O. Mitrofanov, D. V. Lang, C. Kloc, J. M. Wikberg, T. Siegrist, W.-Y. So, M. A. Sergent, and A. P. Ramirez, *Phys. Rev. Lett.* **97**, 166601 (2006).

- [7] H. Najafov, I. Biaggio, V. Podzorov, M.F. Calhoun, and M.E. Gershenson, *Phys. Rev. Lett.* **96**, 056604 (2006).
- [8] H. Najafov, B. Lee, Q. Zhou, L.C. Feldman, and V. Podzorov, *Nature Mater.* **9**, 938 (2010).
- [9] D.A. da Silva Filho, E.-G. Kim, and J.-L. Brédas, *Adv. Mater.* **17**, 1072 (2005).
- [10] Y. Xia, V. Kalihari, C.D. Frisbie, N.K. Oh, and J.A. Rogers, *Appl. Phys. Lett.* **90**, 162106 (2007).
- [11] H. Nishimura, T. Yamaoka, A. Matsui, K. Mizuno, and G.J. Sloan, *J. Phys. Soc. Jpn.* **54**, 1627 (1985).
- [12] M. Voigt, A. Langner, P. Schouwink, J.M. Lupton, R.F. Mahrt, and M. Sokolowski, *J. Chem. Phys.* **127**, 114705 (2007); A. Camposeo, M. Polo, S. Tavazzi, L. Silvestri, P. Spearman, R. Cingolani, and D. Pisignano, *Phys. Rev. B* **81**, 033306 (2010).
- [13] S. Tao, H. Matsuzaki, H. Uemura, H. Yada, T. Uemura, J. Takeya, T. Hasegawa, and H. Okamoto, *Phys. Rev. B* **83**, 075204 (2011).
- [14] N. Geacintov and M. Pope, *J. Chem. Phys.* **50**, 814 (1969).
- [15] M. Pope and C. Swenberg, *Electronic Processes in Organic Crystals and Polymers* (Oxford University Press, Oxford, 1999).
- [16] See Supplemental Material at <http://link.aps.org/supplemental/10.1103/PhysRevLett.109.097403> for the details of the PL spectrum.
- [17] A. Saeki, S. Seki, T. Takenobu, Y. Iwasa, and S. Tagawa, *Adv. Mater.* **20**, 920 (2008).
- [18] J.-F. Chang, T. Sakanoue, Y. Olivier, T. Uemura, M.-B. Dufourg-Madec, S.G. Yeates, J. Cornil, J. Takeya, A. Troisi, and H. Sirringhaus, *Phys. Rev. Lett.* **107**, 066601 (2011).
- [19] H.J. Zeiger, J. Vidal, T.K. Cheng, E.P. Ippen, G. Dresselhaus, and M.S. Dresselhaus, *Phys. Rev. B* **45**, 768 (1992).
- [20] L. Dhar, J.A. Rogers, and K.A. Nelson, *Chem. Rev.* **94**, 157 (1994).
- [21] J.R. Weinberg-Wolf, L.E. McNeil, S. Liu, and C. Kloc, *J. Phys. Condens. Matter* **19**, 276204 (2007).
- [22] B.A. West, J.M. Womick, L.E. McNeil, K.J. Tan, and A.M. Moran, *J. Phys. Chem. C* **114**, 10580 (2010).
- [23] E. Venuti, I. Bilotti, R.G. Della Valle, and A. Brillante, *J. Phys. Chem. C* **112**, 17416 (2008).
- [24] L. Huang, Q. Liao, Q. Shi, H. Fu, J. Ma, and J. Yao, *J. Mater. Chem.* **20**, 159 (2010).
- [25] A. Ryasnyanskiy and I. Biaggio, *Phys. Rev. B* **84**, 193203 (2011).
- [26] P. Irkhin and I. Biaggio, *Phys. Rev. Lett.* **107**, 017402 (2011).
- [27] V.K. Thorsmølle, R.D. Averitt, J. Demsar, D.L. Smith, S. Tretiak, R.L. Martin, X. Chi, B.K. Crone, A.P. Ramirez, and A.J. Taylor, *Phys. Rev. Lett.* **102**, 017401 (2009).
- [28] If we assume $\tau = 50$ ps and the diffusion length of a triplet is $5 \mu\text{m}$, the diffusion constant is $5000 \text{ cm}^2/\text{s}$, which is not realistic [8].